

EXTENDED CALCULATIONS OF ENERGY LEVELS AND TRANSITION RATES FOR SINGLY IONIZED LANTHANIDE ELEMENTS I: PR - GD

LAIMA RADŽIŪTĖ,¹ GEDIMINAS GAIGALAS,¹ DAJI KATO,² PAVEL RYNKUN,¹ AND MASAOMI TANAKA³

¹*Institute of Theoretical Physics and Astronomy, Vilnius University, Saulėtekio Ave. 3, Lithuania*

²*National Institute for Fusion Science, 322-6 Oroshi-cho, Toki 509-5292, Japan*

³*Astronomical Institute, Tohoku University, Sendai 980-8578, Japan*

(Received April 9, 2024; Revised; Accepted)

Submitted to ApJS

ABSTRACT

Lanthanide elements play important roles as an opacity source in the ejected material from neutron star mergers. Accurate and complete atomic data are necessary to evaluate the opacities and to analyze the observed data. In this paper, we perform extended, *ab-initio* atomic calculations from Pr II (Z=59) to Gd II (Z=64). By using multiconfiguration Dirac-Hartree-Fock and relativistic configuration-interaction methods, implemented in the general-purpose relativistic atomic structure package GRASP2K, we calculate the energy levels and transition data of electric dipole transitions. These computations are based on strategies (with small variations) of Nd II published by Gaigalas et al. (2019). Accuracy of data is evaluated by comparing computed energy levels with the NIST database or other works. For the energy levels, we obtain the average relative accuracy of 8%, 12%, 6%, 8%, and 7% for Pr II, Pm II, Sm II, Eu II, and Gd II ions, respectively as compared with the NIST data. Accuracy of energy transfer to the wavelength as 3%, 14% and 11% for Pr II, Eu II and Gd II. Our computed E1 type transition probabilities are in good agreement with experimental values presented by other authors especially for strong transitions.

Keywords: energy spectra, transition data, opacity, neutron stars

1. INTRODUCTION

Atomic opacities of heavy elements have a wide impact to astrophysics. In particular, recent observations of gravitational waves and electromagnetic waves from a neutron star merger (GW170817, [Abbott et al. 2017](#)) highlight the needs for heavy-element opacities. In optical and infrared wavelengths, the electromagnetic counterpart of GW170817 shows characteristics of kilonova, emission powered by radioactive decays of newly synthesized r -process (or rapid neutron capture process) nuclei. To study the r -process nucleosynthesis from the observed emission, we need to accurately understand the opacities of lanthanide elements since properties of kilonova are mainly governed by bound-bound opacities of r -process elements and lanthanide elements give the largest contributions ([Kasen et al. 2013](#); [Barnes & Kasen 2013](#); [Tanaka & Hotokezaka 2013](#)).

Several works have been done to study the properties and opacities of lanthanide elements ([Kasen et al. 2013](#); [Fontes et al. 2017](#); [Tanaka et al. 2018, 2019](#)). However, atomic calculations to evaluate the total opacities are not necessarily accurate enough to give a wavelength and a transition probability of each transition ([Tanaka et al. 2019](#)). Recently, [Watson et al. \(2019\)](#) reported identification of Sr in the spectra of kilonova associated with GW170817. In principle, other elements can also be identified in the spectra. However, the line list used for astrophysics is not necessarily complete even for strong transitions, in particular, in infrared wavelengths. By these reasons, it is still not straightforward to fully decode the spectra of kilonova. Accurate atomic calculations of lanthanide elements, therefore, play an important role as a benchmark to give accurate atomic data ([Gaigalas et al. 2019](#)).

There are many semi-empirical works which provide accurate atomic data of the lanthanide elements. In these works, the Racah-Slater parametric method is used ([Wyart 2011](#)). This method is known to give an excellent agreement between calculated energies using fitted radial parameters and available experimental energies. However, correct level identification of experimental spectra is needed, which is not always available. On the other hand, *ab-initio* methods can provide complete atomic data set without any empirical parameter. Nevertheless, there are few applications of such *ab-initio* methods for lanthanide with spectroscopic accuracy. This is because systematic improvement of subtle correlation effects in complicated atomic structures of open- $4f$ shell is not studied thoroughly.

In our previous paper ([Gaigalas et al. 2019](#)), we have performed accurate calculations for Nd ions. In this paper, we extend our calculations to Pr II,

Pm II, Sm II, Eu II, and Gd II. Namely, we perform energy spectrum computations for states of the following configurations: $[\text{Xe}]4f^N\{6s, 5d, 6p\}$ and $[\text{Xe}]4f^{N-1}\{5d6s, 5d6p, 6s6p, 5d^2\}$ for $N = 3, 5, 6, 7, 8$. We also perform energy spectrum computations for states of $[\text{Xe}]4f^{N+1}$ configuration for Sm II and Eu II, and $[\text{Xe}]4f^{N-1}6s^2$ configuration for Gd II. Levels up to 10 eV are computed since such low-lying energy levels play dominant roles in the opacities in the neutron star merger ejecta at typical temperature of 5,000 K ([Gaigalas et al. 2019](#)). Using these results, electric dipole (E1) transitions data were computed between these states. In this paper, we aim at providing complete atomic data with the overall accuracy of about 10%. This accuracy is not high enough to directly compare with spectroscopic experiments, but it is adequate to evaluate the opacities ("opacity accuracy" rather than "spectroscopic accuracy", [Gaigalas et al. 2019](#)). In fact, typical accuracy of complete atomic calculations ([Kasen et al. 2013](#); [Tanaka et al. 2018](#)) is much lower than the accuracy presented in this paper.

The calculations are done using multiconfiguration Dirac-Hartree-Fock (MCDHF) and relativistic configuration-interaction (RCI) methods ([Grant 2007](#); [Fischer et al. 2016](#)), which are implemented in the general-purpose relativistic atomic structure package GRASP2K ([Jönsson et al. 2013](#)). We employ a strategy similar to the [Gaigalas et al. \(2019\)](#) including electron correlation, which is suitable for series of rare earth ions. For low lying levels, higher accuracy can be achieved using computational schemes including more electron correlations as in [Radžiūtė et al. \(2015\)](#). In addition, there is an advantage in the computation since large computational tasks can be split in to smaller tasks by using this method.

In Section 2, we describe our method and strategy of calculations. Then, we show results of energy level structure and transition probabilities in Sections 3 and 4, respectively. Finally we give summary in Section 5.

2. METHODS

2.1. Computational procedure

The computational methods used in this paper follow the methods used in [Gaigalas et al. \(2019\)](#). Therefore, we briefly outline the methods in this section. We refer the reader to ([Fischer et al. 2016](#)) for further details. We use the MCDHF method, based on Dirac-Coulomb Hamiltonian, in this work. The atomic state functions (ASFs) are expressed by a linear combination of symmetry adapted configuration state functions (CSFs). The CSFs are built from products of one-electron Dirac orbitals. The radial parts of the Dirac orbitals and the

expansion coefficients are optimized to self-consistency in the relativistic self-consistent field procedure.

The spin-angular approach (Gaigalas & Rudzikas 1996; Gaigalas et al. 1997) is used in these computations. The approach is based on the second quantization in a coupled tensorial form, on the angular momentum theory in the orbital, spin, and quasispin spaces and on the reduced coefficients of fractional parentage. It allows us to study configurations with open f -shells without any restrictions.

Table 1. Summary of Computed Levels and Active Space Size.

Ion	Number of levels		N_{CSFs}	
	Even	Odd	Even	Odd
Pr II	927	1 218	29 129	45 045
Nd II*	3 270	2 813	188 357	113 900
Pm II	5 206	4 568	380 588	518 957
Sm II	3 153	5 240	1 272 634	2 133 183
Eu II	1 306	1 241	1 501 949	2 201 859
Gd II	2 035	2 335	3 033 793	1 721 371

NOTE—* Nd II data are published in (Gaigalas et al. 2019).

In the following RCI calculations, the Breit interaction is included in the Hamiltonian. In the RCI calculation, the leading quantum electrodynamics corrections (QED), self-interaction and vacuum polarization are also included.

The label of the ASF is the same as the label of the dominating CSF. The ASFs are obtained as expansions over jj -coupled CSFs. To provide the ASFs in the LSJ labeling system, transformation from a jj -coupled CSF basis to an LSJ -coupled CSF basis has been done (Gaigalas et al. 2017). Review on all these methods and on the GRASP2K package can be found in Fischer et al. (2016).

2.2. Computation of transition probabilities

For electric dipole transitions there are two forms of the transition operator: the length (Babushkin) and velocity (Coulomb) forms. Although the exact solutions of the Dirac-equation should give the same value of the transition moment (Grant 1974), they do not necessarily agree in numerical calculations. The quantity $dT = |A_1 - A_v|/\max(A_1, A_v)$ (Ekman et al. 2014) defines

the accuracy of the computed transition rates, where A_1 and A_v are the transition rates in length and velocity forms, respectively.

The calculation of the transition moment breaks down in the task of summing up reduced matrix elements between different CSFs. Using standard techniques, by assuming that both left and right hand CSFs are formed from the same orthonormal set of spin-orbitals, the reduced matrix elements can be evaluated. This constraint is severe, since a high-quality and compact wave function requires orbitals optimized for a specific electronic state (see for example Fritzsche & Grant 1994). To avoid the problems of having a single orthonormal set of spin-orbitals, the wave-function representations of the two states are transformed in a way that the orbital sets became biorthonormal (Olsen et al. 1995). To evaluate the matrix elements of the transformed CSFs, standard methods as in Fischer et al. (2016) are used.

2.3. Computational Schemes

To compute singly ionized lanthanide elements, the **strategy C** by Gaigalas et al. (2019) is used. Details of this strategy and extension of it are given below. Active space method is used for computation of energy levels and E1 transitions. The configuration space is increased step by step, by increasing the number of layers (L), that is, a set of virtual orbitals. The virtual orbitals of the increased layer are optimized in the relativistic self-consistent field procedure, while all orbitals of inner layers are fixed. The scheme used to increase the active spaces of the CSFs is presented below:

$$AS_{0L} = \{6s, 6p, 5d\},$$

$$AS_{1L} = AS_{0L} + \{7s, 7p, 6d, 5f\},$$

$$AS_{2L} = AS_{1L} + \{8s, 8p, 7d, 6f, 5g\}.$$

The number of computed levels and CSFs in the final even and odd state expansions are presented in Table 1.

Computations are performed for each configuration separately (single reference method). This method allows to split the large computations into several tasks. In each task, the wave function expansion for a single reference configuration is constructed by substitution of one and two electrons from the reference configuration. For configurations $4f^N 6s$, $4f^N 6p$ and $4f^N 5d$, single and/or double (SD) substitutions are allowed from $4f^N nl$ shells ($l = s, p, d$) to $AS_{0L,1L}$ and single (S) substitutions are allowed to AS_{2L} . For configurations $4f^{N-1} 5d 6s$, $4f^{N-1} 5d 6p$, $4f^{N-1} 6s 6p$, and $4f^{N-1} 5d^2$, only S substitutions are allowed. For Sm II and Eu II ions, a new configuration $4f^{N+1}$, which was not taken into account in the **strategy C** of Gaigalas et al. (2019), is computed. For this configuration, single, double, and triple (SDT) substitutions are allowed from $4f^{N+1}$ shell

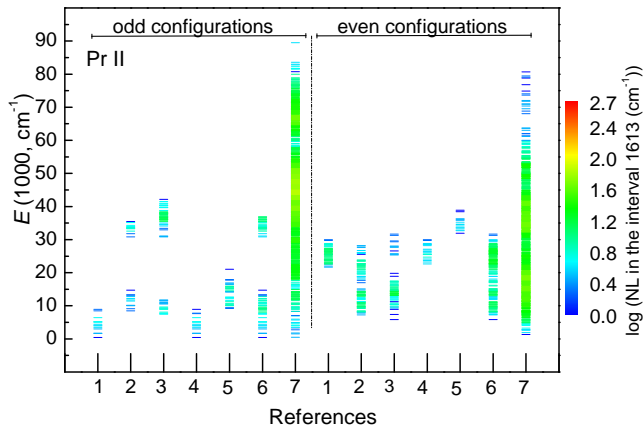


Figure 1. Comparison of energy levels for odd and even configurations of Pr II with experimental values. References (1) Rosen et al. (1941); (2) Blaise et al. (1973) and Blaise et al. (1974); (3) Ginibre (1989a); (4) Ivarsson et al. (2001); (5) Furmann et al. (2001), Furmann et al. (2005) and Furmann et al. (2007); (6) Akhtar & Windholz (2019); (7) Our computed levels. NL is the number of levels.

to $AS_{0L,1L}$ and SD substitutions are allowed to AS_{2L} . For configuration $4f^{N-1}nl n'l'$, two electrons are excited from $4f$ orbital, and for $4f^N nl$, only one electron is excited from $4f$ orbital. Therefore, to include compensated correlations, we need to make less excitations from the first configuration and more excitations from the second one. For example, if we do SD substitutions for $4f^{N-1}nl n'l'$ configuration, we need to make SDT substitutions for $4f^N nl$ configuration.

To compute energy levels, it is important to have correct core radial wave functions, that is, initial Dirac-Fock (DF) computations. Correct selection of the core stabilizes solution of self-consistent field computation. We find that core radial wave functions $[Xe]4f$ from the ground configuration $[Xe]4f^N 6s$ are the best solution. Radial wave functions up to $4f, 5s, 5p$ orbital are taken from the ground configuration for these configurations $4f^{N-1}5d6s$, $4f^{N-1}5d6p$, $4f^{N-1}6s6p$, and $4f^{N-1}5d^2$. Meanwhile, the radial wave functions were computed for each configurations $4f^N nl$ ($l = s, p, d$) separately.

For neutral atoms and ions of lanthanide elements with different ground configurations, we suggest that their ground configuration radial wave functions are used as common core. For example, for neutral lanthanides, radial wave functions of the ground configurations $[Xe]4f^N 6s^2$ can be used as common core.

For Eu II and Gd II, wave function is investigated differently due to the rapid increase of the number of configuration state functions in the active space (see Table 1). For these ions, self-consistent field computations are performed not for all J values but only for

one J value. Then, using computed radial wave functions, RCI computations are performed. For example, for the configuration of Eu, $4f^5 6s$ atomic states only with $J = 4$ are computed and it is later used in the RCI computation for $J = 0 - 13$. For all configurations, the lowest J values are selected for computation of the radial wave functions. This computational method demands less computational resources.

In addition, some states of Rydberg series (up to 10 eV) are computed for Eu II. This includes 38 levels from configurations $4f^6\{7s, 8s, 6d, 7d, 7p, 8p\}$. Radial wave functions for configurations $4f^6\{7s, 8s\}$ up to $4f$ are taken from the ground configuration ($4f^6 6s$). For the rest configurations, radial wave functions are computed in the same manner as in the configurations $4f^6\{5d, 6p\}$. This means that each configuration from $4f^6\{6d, 7d, 7p, 8p\}$ has different radial wave functions. Active space generated in a similar manner as for the configurations $4f^6\{6s, 5d, 6p\}$. For example, active space for the configuration are generated by SD substitutions from $4f^6 8s$ to $AS_{0L} = \{6p, 5d\}$ and $AS_{1L} = AS_{0L} + \{6s, 7p, 6d, 5f\}$ and by S substitutions to $AS_{2L} = AS_{1L} + \{7s, 8p, 7d, 6f, 5g\}$.

For Gd II, radial wave function is generated also for only one J value. Radial wave functions of $4f^7 5d^2$, $4f^7 6s^2$, $4f^7 5d6s$, and $4f^8 6p$ are computed together, using radial wave function of configuration $4f^8 6s$ up to $4f$. Rest of configurations are computed in the same manner as for Eu II. The MCDHF calculations are then followed by RCI calculations by including the Breit interaction and leading QED effects. The same active space (AS_{2L}) is used for the RCI computations as well as for MCDHF computations.

3. ENERGY LEVELS

All levels for $Z = 59 - 64$ ions are given in Figure 2, and the energy data computed for Pr II, Pm II, Sm II, Eu II, and Gd II are given in machine-readable format in Tables 4, 5, 6, 7, and 8, respectively. This includes label, J and P values, and energy value. Levels are given in LS -coupling, although it is suitable only for the lowest states of configurations and determination the configuration is complicated for higher states (Cowan 1981). For the labels, we use notation $4f^N_{Nr} (2S+1)L n'l' (2S'+1)L'$. Intermediate quantum numbers define parent levels $4f^N_{Nr} (2S+1)L$, where N is electron number in $4f$ shell, $(2S+1)$ is multiplicity, Nr is a sequential index number representing the group labels nWU for the term, and L is orbital quantum number (see Gaigalas & Rudzikas 1998 for more about Nr). More complicated configurations are presented in the similar way.

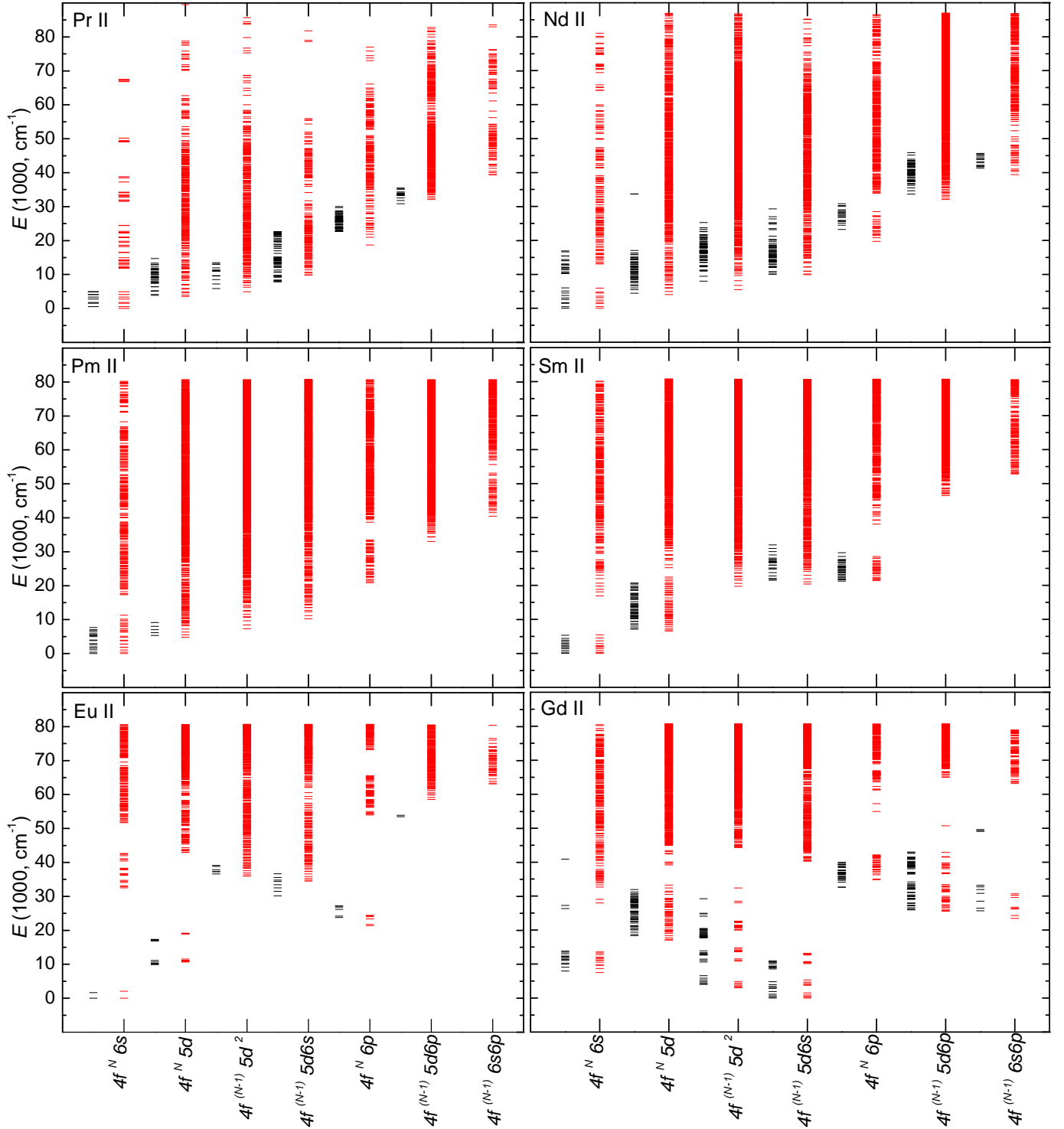


Figure 2. Energy levels for configurations of Pr II - Gd II are compared with data in the NIST database. Energy levels with questionable identification in the NIST database also included. Black lines represent the NIST data while red lines represent all computed energy levels. Nd II data are published in (Gaigalas et al. 2019). N is the number of electrons in the $4f$ shell ($N = 3 - 8$ for Pr II, Nd II, Pm II, Sm II, Eu II and Gd II respectively).

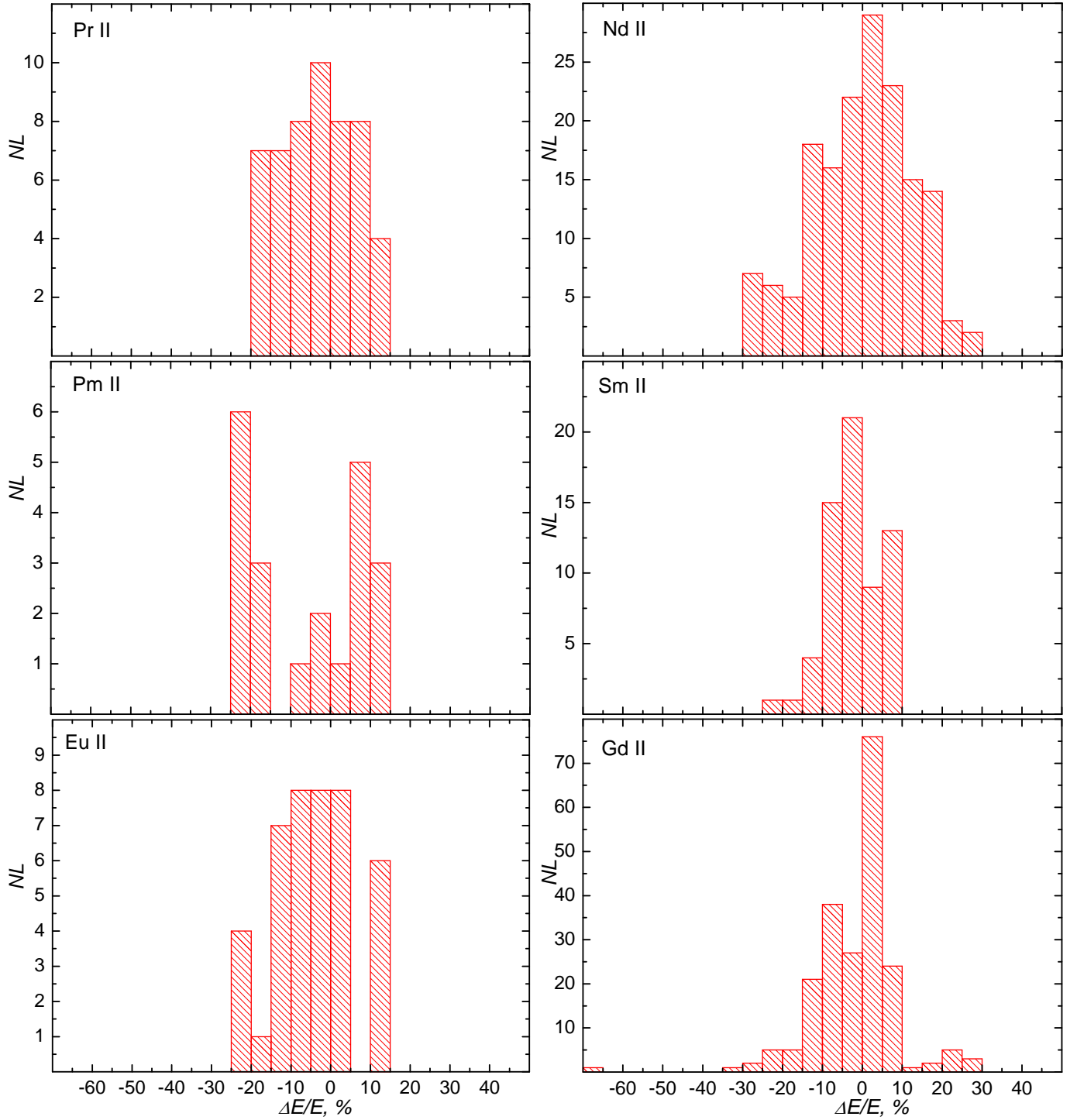


Figure 3. Histogram of the relative accuracy with respect to the NIST data ($\Delta E_i/E_{\text{NIST}} = (E_{\text{NIST}} - E_i)/E_{\text{NIST}} \times 100\%$) for Pr II - Gd II. Nd II data are published in [Gaigalas et al. \(2019\)](#). NL is number of levels.

Table 2. Comparison of Energy Levels with the NIST Database, $\overline{\Delta E/E}$ (in %) and the Number of Compared Levels (NL).

	Pr II		Nd II		Pm II		Sm II		Eu II		Gd II	
	$\overline{\Delta E/E}$	NL	$\overline{\Delta E/E}$	NL	$\overline{\Delta E/E}$	NL	$\overline{\Delta E/E}$	NL	$\overline{\Delta E/E}$	NL	$\overline{\Delta E/E}$	NL
$4f^N 6s$	6	7	15	27	13	17	8	12	23	1	4	13
$4f^N 6p$	4	12	13	23	-	-	-	-	10	6	6	30
$4f^N 5d$	10	33	8	47	10	5	5	52	9	10	3	56
$4f^{N-1} 5d 6s$	-	-	2	14	-	-	-	-	15	8	19	19
$4f^{N-1} 5d 6p$	-	-	6	12	-	-	-	-	-	-	2	49
$4f^{N-1} 6s 6p$	-	-	4	13	-	-	-	-	-	-	8	6
$4f^{N-1} 5d^2$	15	1	15	22	-	-	-	-	13	3	13	39
$4f^{N-1} 6s^2$											66	1
$4f^{N+1}$							14	1	-	-		
$4f^N 7s$									3	2		
$4f^N 8s$									9	1		
$4f^N 6d$									2	10		
all	8	53	10	158	12	22	6	65	8	41	7	213

NOTE—* Nd II data are published in [Gaigalas et al. \(2019\)](#). Levels with unquestionable identification are included in to the comparison.

To evaluate the accuracy of our calculations, comparison with critically evaluated data is necessary. In this section, we first summarize the available data for energy levels of Pr II, Pm II, Sm II, Eu II, Gd II in the NIST database. Then, we compare calculated energy levels with these available data.

3.1. Available data

3.1.1. Pr II

[Ginibre \(1989a\)](#) have investigated 105 odd and 187 even experimental energies based on Fourier transform (FT) spectroscopy in range 2 783 - 27 920 cm^{-1} . Also, the large amount levels were investigated by [Rosen et al. \(1941\)](#), [Blaise et al. \(1973\)](#), and [Blaise et al. \(1974\)](#). They performed semi-empirical fitting procedure to assign for some levels labels in *LS*-coupling ([Ginibre 1989b](#)). Later, [Ivarsson et al. \(2001\)](#) presented improved 39 energy levels using FT spectroscopy in 2 800 - 8 000 \AA region. [Furmann et al. \(2001, 2005, 2007\)](#) investigated 31 odd and 14 even levels, using laser-induced fluorescence spectroscopy (LIF) in a hollow cathode discharge lamp. More recently, [Akhtar & Windholz \(2019\)](#) have redetermined energy values of 227 levels (74 having odd and 153 even parity) and hyperfine structures of 477 transitions in the range of 3 260 - 11 700 \AA . They

corrected the energy levels from the works of [Ginibre \(1989a\)](#) and [Ivarsson et al. \(2001\)](#).

All of these levels are measured/reanalyzed in high accuracy. However, each work presents energy levels in a narrow range as shown in Figure 1. Therefore, the transitions between measured energy levels give too small amount of lines needed for computation of opacities in neutron star mergers. Data of these authors are summarized by [Martin et al. \(1978\)](#). Since the NIST database ([Kramida et al. 2018](#)) includes the work by ([Martin et al. 1978](#)), we only give comparison with the NIST database here.

3.1.2. Pm II

Pm II is one of the ions whose spectrum is not well investigated. Energy levels of two configurations $4f^5 6s$ and $4f^5 5d$ were investigated by [Martin et al. \(1978\)](#). Five new levels of $4f^5 5d$ configuration were measured by [Ottot et al. \(1995\)](#) with the collinear laser ion beam spectroscopy (CLIBS) method and were identified using Hartree-Fock method.

3.1.3. Sm II

[Albertson \(1936\)](#) have assigned terms of 40 even levels of the $4f^6 6s$ and $4f^6 5d$ configurations based on the

Zeeman patterns of over 300 lines. Spector (1970a) have done semi-empirical computation of energy values and LS -composition of 55 levels for $4f^6(^7F)5d$ configuration. Also, a large amount of work for energy levels was done by Blaise et al. (1969): 325 levels for Sm II were obtained from the Zeeman effect measurement in the visible and the ultraviolet spectrum. Then, these energy levels were re-evaluated by Martin et al. (1978). Attempt of identification of odd configurations for some levels was done by Rao et al. (1990) using isotope shifts data, which was carried out on a recording Fabry-Perot spectrometer. The hyperfine structure and isotope shift were also measured by collinear fast ion beam laser spectroscopy. These data were used to assign configurations to the 13 odd upper levels by Villemoes et al. (1995). Note that some of them do not have identification by Martin et al. (1978).

3.1.4. Eu II

156 levels of configurations $4f^7\{6s, 7s, 8s, 5d, 6d, 6p\}$ and $4f^65d6s$, $4f^65d^2$ were resolved with the spark spectrum of arc by Russel et al. (1941). This work is the extension of the analysis by Albertson (1934) on 9 levels of $4f^7\{6s, 5d, 6p\}$ configurations. Then these energy levels were re-evaluated by Martin et al. (1978). More recently, 13 new energy levels of $4f^76s$ configuration were suggested from hyperfine constant and isotope shift measurements (Furmann & Stefańska 2013).

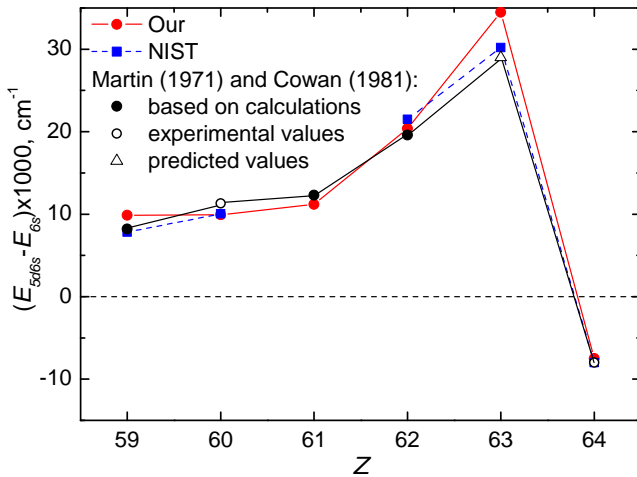


Figure 4. The difference between the lowest level of $4f^{N-1}5d6s$ and the lowest level of $4f^N6s$ for singly ionized lanthanide elements. Red circles are our computed theoretical values, while blue squares are values recommended by the NIST database. Black symbols indicate data from Martin (1971) and Cowan (1981): closed circles are predicted values, open circles are experimental values, and triangles are estimated data based on incomplete experimental data.

3.1.5. Gd II

Albertson et al. (1940) have investigated 9 odd and 11 even energy levels, have deduced quantum numbers from Zeeman effect pattern, and have established the ground configurations to be $4f^75d6s$. Venugopalan et al. (1998) and Ahmad et al. (1979) have measured isotope shift of 33 spectroscopic lines, using photoelectric recording Fabry-Perot spectrometer. They suggested new configuration identification of 4 high energy levels (lying above $35\,000\text{ cm}^{-1}$): $35\,362.630\text{ cm}^{-1}$ ($J = 13/2$) as $4f^75d6s$; $35\,822.697\text{ cm}^{-1}$ ($J = 9/2$) as mix of two configurations $4f^75d6s + 4f^86p$; $37\,831.032\text{ cm}^{-1}$ ($J = 11/2$) and $38\,010.603\text{ cm}^{-1}$ ($J = 11/2$) as $4f^86p$. Blaise et al. (1971) have done the analysis of the spark spectrum of Gd II of 178 new levels. Total 30 levels were ascribed to $4f^8(^7F)6p$ configuration by their strong transitions with the levels on the $4f^8(^7F)6s$ and $4f^8(^7F)5d$ sub-configurations. Spector (1970a) have done semi-empirical computation of energy values and LS -composition of 57 levels for $4f^8(^7F)5d$ configuration. 164 odd and 150 even parity energy levels of Gd II are listed by Martin et al. (1978). Spector (1970b) have done extended analysis on levels of the configurations $4f^8(^7F)\{6s, 6p, 5d\}$ and measured new levels of $4f^8(^7F)\{6s, 5d\}$ configurations and new odd levels.

3.2. Comparison of the energy levels

The energy levels for each configuration are compared with those in the NIST database in Figure 2. Only the common configurations for Pr II - Gd II are presented in the figure. Although the energy levels in the NIST database sometimes include questionable identification of the configuration, this figure includes all levels.

To analyse the accuracy of our calculations as compared with the NIST data, we use an expression $\Delta E_i/E_{\text{NIST}} = (E_{\text{NIST}} - E_i)/E_{\text{NIST}} \times 100\%$. For the indicator of the accuracy for many levels, we use a value $\Delta E/\bar{E} = \sum \frac{|\Delta E_i/E_{\text{NIST}}|}{N}$, where N is the number of the compared levels. Summary of the accuracy for each configuration is given in Table 2. Levels with unquestionable identification are included in to the comparison. Empty space in Table 2 means that configuration is not computed while a mark with "-" means that data are missing in the NIST database (or there is only one level). The last line (all) of the table presents averaged accuracy with unquestionable identification between our results and the NIST database.

Overall, we find that our calculations give good accuracy: 8%, 12%, 6%, 8%, and 7% for Pr II, Pm II, Sm II, Eu II, and Gd II ions, respectively. There is no clear trend with the atomic number Z . The accuracy depends on the configurations. For example, the degree

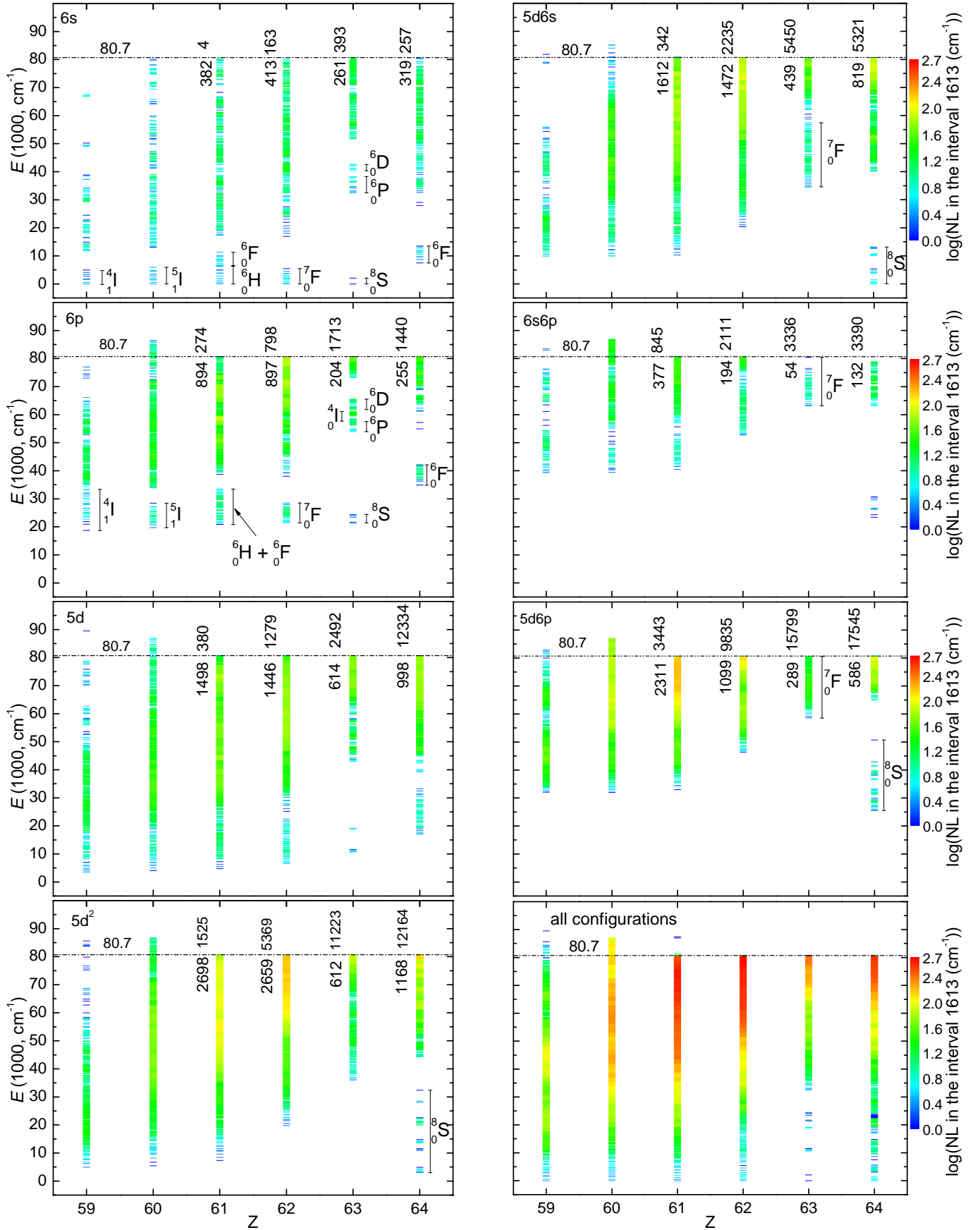


Figure 5. Energy level density and structure of $4f^N\{6s, 6p, 5d\}$, $4f^{N-1}\{5d6s, 5d6p, 6s6p\}$, and $4f^{N-1}5d^2$ configurations and all levels for the ions with $Z = 59 - 64$. The blocks of levels and the corresponding parent levels are also given. NL is the number of levels. The horizontal lines show our energy threshold (10 eV), and the numbers above/below the lines show the number of levels above/below this threshold.

Table 3. Singly Ionized Atom Ground State Orbitals Radii (a.u.) for Lanthanide $Z = 59 - 64$ Compared with those by Indelicato et al. (2007)[I07].

Ion	$\langle 4f_- \rangle$	$\langle 4f \rangle$	$\langle 5d_- \rangle$	$\langle 5d \rangle$	$\langle 6s \rangle$
Pr II	1.0833	1.0986	2.5036	2.5484	4.3130
I07	1.0589	1.0667			4.2924
Nd II*	1.0291	1.0440	2.4607	2.5085	4.2522
I07	1.0054	1.0190			4.2252
Pm II	0.9832	0.9981	2.4223	2.4717	4.1948
I07	0.9624	0.9796			4.1608
Sm II	0.9442	0.9590	2.3892	2.4400	4.1402
I07	0.9249	0.9392			4.1012
Eu II	0.9098	0.9256	2.3642	2.4272	4.0870
I07	0.8920	0.8999			4.0438
Gd II	0.8797	0.8929	2.3991	2.5041	3.6878
I07	0.8218	0.8221	2.4547	2.4846	3.7930

NOTE—* Orbital radii of Nd II were computed during MCDHF computations in Gaigalas et al. (2019), but have not been unpublished.

of agreement for $4f^N 6s$, $4f^N 5d$ and $4f^N 6p$ configurations slightly differ. These variations of the differences is mainly caused by the different number of levels used for comparison. Note that the biggest deviation is found for level $^8S_{7/2}$ of configuration $4f^7 6s^2$ (66% difference for this 1 level).

As mentioned in Section 2.3, computations of Eu II are performed in a slightly different manner: radial wave functions are computed only for one J symmetry of the lowest ASF. To test the influence of such splitting, we compute configurations $4f^7 6s$, $4f^7 5d$, $4f^6 5d 6s$, $4f^6 5d 6p$, and $4f^6 5d^2$ in both ways. We find that the differences between two methods are small: the maximum averaged difference of energy levels per configuration is 0.5% for $4f^7 5d$ configuration (614 levels) and the minimum difference is 0.02% for $4f^7 6s$ (261 levels). Levels of Rydberg state of the configurations $4f^7 \{7s, 8s, 6d\}$ for Eu II are also compared in Table 2. There is a good agreement for levels of configurations $4f^7 \{7s, 6d\}$ obtained in this research with values from NIST database.

Figure 3 show the histogram of the relative difference compared to the NIST for all computed ions. This figure includes only the levels with the exact identification. Note that the number of the available energy levels has a large variation as summarized in Section 3.1. The

Table 4. Energy Levels (in cm^{-1}) Relative to the Ground State for the States of Pr II.

No.	label	J	P	E
1	$4f^3(^4I) 6s^5I$	4	—	0.00
2	$4f^3(^4I) 6s^5I$	5	—	511.12
3	$4f^3(^4I) 6s^5I$	6	—	1558.26
4	$4f^3(^4I) 6s^3I$	5	—	1772.15
5	$4f^3(^4I) 6s^5I$	7	—	2773.88
6	$4f^3(^4I) 6s^3I$	6	—	3337.17
7	$4f^3(^4I) 5d^5L$	6	—	3506.00
8	$4f^3(^4I) 5d^5K$	5	—	3948.78
9	$4f^3(^4I) 6s^5I$	8	—	4104.37
10	$4f^3(^4I) 5d^5L$	7	—	4553.26
11	$4f^3(^4I) 5d^5K$	6	—	4898.65
12	$4f^3(^4I) 6s^3I$	7	—	4937.25
13	$4f^2(^3H) 5d^2(^3F)^5L$	6	+	4948.47
14	$4f^3(^4I) 5d^5L$	8	—	5703.77
15	$4f^3(^4I) 5d^5K$	7	—	5941.26
16	$4f^2(^3H) 5d^2(^3F)^5L$	7	+	6265.05
17	$4f^2(^3H) 5d^2(^3F)^5I$	4	+	6861.72
18	$4f^3(^4I) 5d^5L$	9	—	6944.26
19	$4f^3(^4I) 5d^5K$	8	—	7067.68
20	$4f^2(^3H) 5d^2(^3F)^5K$	5	+	7591.81

NOTE— Table 4 is published in its entirety in the machine-readable format. Part of the values are shown here for guidance regarding its form and content.

biggest numbers of levels are available for the Nd II and the Gd II in the NIST database, and thus, the distribution is close to the normal distribution for these ions.

The accuracy of our calculations can also be evaluated using Figure 4, which shows the energy difference between the lowest levels of $4f^{N-1} 5d 6s$ and the lowest levels of $4f^N 6s$ configurations for singly ionized lanthanides. As shown in the figure, the overall agreement is very good. Our results and those in the NIST database give smaller energy differences than those in Martin (1971) and Cowan (1981) for Nd II and Pm II ions. The increase of the energy difference is observed for Eu II by all the works, but our result shows a bigger increase than in Martin (1971), Cowan (1981) and the NIST data.

Here it should be noted that, for the cases of Pr II and Sm II, the identification of $4f^{N-1} 5d 6s$ configurations are questionable in the NIST database. More detailed investigation was done by Brewer (1971) (see their Figure 1). They have estimated energies for lowest levels

Table 5. Energy Levels (in cm⁻¹) Relative to the Ground State for the States of Pm II.

No.	label	<i>J</i>	P	<i>E</i>
1	$4f^5({}^6H) 6s {}^7H$	2	—	0.00
2	$4f^5({}^6H) 6s {}^7H$	3	—	441.78
3	$4f^5({}^6H) 6s {}^7H$	4	—	1073.15
4	$4f^5({}^6H) 6s {}^5H$	3	—	1850.51
5	$4f^5({}^6H) 6s {}^7H$	5	—	1858.38
6	$4f^5({}^6H) 6s {}^7H$	6	—	2765.09
7	$4f^5({}^6H) 6s {}^5H$	4	—	2830.31
8	$4f^5({}^6H) 6s {}^7H$	7	—	3765.53
9	$4f^5({}^6H) 6s {}^5H$	5	—	3914.91
10	$4f^5({}^6H) 5d {}^7K$	4	—	4799.46
11	$4f^5({}^6H) 6s {}^7H$	8	—	4836.02
12	$4f^5({}^6H) 6s {}^5H$	6	—	5078.38
13	$4f^5({}^6H) 5d {}^7K$	5	—	5507.08
14	$4f^5({}^6H) 6s {}^5H$	7	—	6298.26
15	$4f^5({}^6H) 5d {}^7K$	6	—	6322.77
16	$4f^5({}^6F) 6s {}^7F$	0	—	6567.93
17	$4f^5({}^6F) 6s {}^7F$	1	—	6678.52
18	$4f^5({}^6F) 6s {}^7F$	2	—	6917.29
19	$4f^5({}^6H) 5d {}^7K$	7	—	7232.66
20	$4f^5({}^6F) 6s {}^7F$	3	—	7320.95

NOTE—Table 5 is published in its entirety in the machine-readable format. Part of the values are shown here for guidance regarding its form and content.

of configurations involving $4f$, $5d$, $6p$, and $6s$ shells for singly-triply ionized lanthanides and actinides. Their computations are based on the thermodynamic data of the metals. In a similar manner, the energy differences were also analysed by Vander Sluis & Nugent (1974). In fact, our results are very close to the data of these authors.

3.3. Energy level distribution for each configuration

Identification of energy levels is a complicated task for lanthanides due to a mix of configurations. Even assigning particular configuration labeling to some levels is complicated. The discussion below should give enlightenment on the inner structure of the energy spectrum. Energy levels have formed groups around parent level of $4f^N$ or $4f^{N-1}$ configurations with the same term of f shell. Levels belonging to the different groups are separated by energy gaps. Below are given more details about these groups for each configuration.

Energy level structures for states of $4f^N\{6s, 6p, 5d\}$, $4f^{N-1}\{5d6s, 5d6p, 6s6p\}$, and $4f^{N-1}5d^2$ configurations are presented in Figure 5. Cut off line 80 700 cm⁻¹ (10 eV) is given by the horizontal lines. For the Pr II and Nd II, computations are done up to ionizations limits: it is 85 745 cm⁻¹ for Pr II and 86 970 cm⁻¹ for Nd II according to the NIST database. The number of computed levels are displayed below the line and the number of levels above the line are left uncomputed. The sum of these numbers comprise a possible number of levels in jj -coupling. We find that the increase of the nuclear charge has a small effect on the positions of first level relative to the ground state for the configurations $4f^N 6p$ and $4f^N 5d$. The energy level structures of these configurations are influenced by the structure of core $[\text{Xe}]4f^N$. Similar to the system difference analysed by Cowan (1981), the increase of the energy of first level relative to the ground state is found for the configurations of $4f^{N-1}5d6s$, $4f^{N-1}5d6p$, $4f^{N-1}6s6p$, and $4f^{N-1}5d^2$ (see Figure 4 for $4f^{N-1}5d6s$). The highest density of the energy levels are found for $4f^{N-1}5d^2$ and $4f^{N-1}5d6p$ configurations.

The lowest levels of $4f^N 6s$ and $4f^N 6p$ configuration form blocks of energy levels around the parent levels of $4f^N$ (${}^4I^*$, ${}^5I^*$, 6H and ${}^6F^*$), (${}^7F^*$), (${}^8S^*$, 6P , ${}^6I^*$, and ${}^6D^*$), and (${}^7F^*$) for $Z = 59-64$, respectively. After the levels with core configuration marked by “*” above, there is an energy gap, except for $4f^3 6p$ of Pr II ion. Levels with the specific parent levels do not mix with others, except for the parent level states of $4f^5 6p$ of Pm II ion ($4f^5 {}^6H$ mix between $4f^5 {}^6F^*$). For $4f^N 5d$ configuration, the situation is different because of the strong interaction between $4f$ and $5d$ (Figure 5).

For $4f^{N-1}5d6s$ configuration, groups of energy levels are formed around the lowest parent levels for only two elements i.e., Eu II and Gd II. These parent levels are $4f^6 {}^7F$ and $4f^7 {}^8S^*$ for Eu II and Gd II, respectively. For $4f^{N-1}5d6p$ configuration, only for Gd II has formed a group of energy levels around $4f^7 {}^8S^*$ parent level (Figure 5).

Levels of $4f^{N-1}6s6p$ configuration do not form group of energy levels around the parent levels. For Eu II, all levels of $4f^6 6s6p$ and of $4f^6 5d6p$ configurations belong to the parent levels $4f^6 {}^7F$, because of the 10 eV cut off (Figure 5). For $4f^{N-1}5d^2$ configuration, groups of energy levels forms around the lowest parent levels for Gd II $4f^8 {}^8S^*$ (Figure 5).

Radii of the orbitals of the configuration $4f^N 6s$ and $4f^{N-1}5d6s$ are presented in Table 3. For higher Z , all orbitals contract (see Table 3). The exception is Eu II and Gd II: there is no big differences for $< 5d_- >$ and $< 5d >$ orbitals between Eu II and Gd II. Indeed, for

Table 6. Energy Levels (in cm^{-1}) Relative to the Ground State for the States of Sm II.

No.	label	J	P	E
1	$4f^6(\frac{7}{0}F) 6s^8F$	1/2	+	0.00
2	$4f^6(\frac{7}{0}F) 6s^8F$	3/2	+	296.55
3	$4f^6(\frac{7}{0}F) 6s^8F$	5/2	+	765.67
4	$4f^6(\frac{7}{0}F) 6s^8F$	7/2	+	1372.98
5	$4f^6(\frac{7}{0}F) 6s^6F$	1/2	+	1853.48
6	$4f^6(\frac{7}{0}F) 6s^8F$	9/2	+	2084.20
7	$4f^6(\frac{7}{0}F) 6s^6F$	3/2	+	2285.57
8	$4f^6(\frac{7}{0}F) 6s^8F$	11/2	+	2870.66
9	$4f^6(\frac{7}{0}F) 6s^6F$	5/2	+	2918.77
10	$4f^6(\frac{7}{0}F) 6s^6F$	7/2	+	3688.53
11	$4f^6(\frac{7}{0}F) 6s^8F$	13/2	+	3709.70
12	$4f^6(\frac{7}{0}F) 6s^6F$	9/2	+	4548.72
13	$4f^6(\frac{7}{0}F) 6s^6F$	11/2	+	5467.12
14	$4f^6(\frac{7}{0}F) 5d^8H$	3/2	+	6571.55
15	$4f^6(\frac{7}{0}F) 5d^8H$	5/2	+	6913.83
16	$4f^6(\frac{7}{0}F) 5d^8H$	7/2	+	7375.65
17	$4f^6(\frac{7}{0}F) 5d^8H$	9/2	+	7942.79
18	$4f^6(\frac{7}{0}F) 5d^8D$	3/2	+	8488.11
19	$4f^6(\frac{7}{0}F) 5d^8H$	11/2	+	8600.85
20	$4f^6(\frac{7}{0}F) 5d^8D$	5/2	+	9058.38

NOTE— Table 6 is published in its entirety in the machine-readable format. Part of the values are shown here for guidance regarding its form and content.

Table 7. Energy Levels (in cm^{-1}) Relative to the Ground State for the States of Eu II.

No.	label	J	P	E
1	$4f^7(\frac{8}{0}S) 6s^9S$	4	—	0.00
2	$4f^7(\frac{8}{0}S) 6s^7S$	3	—	2057.90
3	$4f^7(\frac{8}{0}S) 5d^9D$	2	—	10657.96
4	$4f^7(\frac{8}{0}S) 5d^9D$	3	—	10784.18
5	$4f^7(\frac{8}{0}S) 5d^9D$	4	—	10964.35
6	$4f^7(\frac{8}{0}S) 5d^9D$	5	—	11212.47
7	$4f^7(\frac{8}{0}S) 5d^9D$	6	—	11551.69
8	$4f^7(\frac{8}{0}S) 5d^7D$	5	—	18922.41
9	$4f^7(\frac{8}{0}S) 5d^7D$	4	—	18964.72
10	$4f^7(\frac{8}{0}S) 5d^7D$	3	—	19032.93
11	$4f^7(\frac{8}{0}S) 5d^7D$	2	—	19095.86
12	$4f^7(\frac{8}{0}S) 5d^7D$	1	—	19143.88
13	$4f^7(\frac{8}{0}S) 6p^9P$	3	+	21378.10
14	$4f^7(\frac{8}{0}S) 6p^9P$	4	+	21708.29
15	$4f^7(\frac{8}{0}S) 6p^9P$	5	+	23385.62
16	$4f^7(\frac{8}{0}S) 6p^7P$	4	+	23999.79
17	$4f^7(\frac{8}{0}S) 6p^7P$	3	+	24276.27
18	$4f^7(\frac{8}{0}S) 6p^7P$	2	+	24446.93
19	$4f^7(\frac{6}{0}P) 6s^7P$	4	—	32530.49
20	$4f^7(\frac{6}{0}P) 6s^7P$	3	—	32852.51

NOTE— Table 7 is published in its entirety in the machine-readable format. Part of the values are shown here for guidance regarding its form and content.

Gd II, the radii for orbitals $< 5d_- >$ and $< 5d >$ show small increase with respect to Eu II. This may be caused by different computation of the radial wave functions (see section 2.3). Some of the radii are compared with computations by Indelicato et al. (2007). Radii by Indelicato et al. (2007) differ from 1 to 8% from those computed in this paper. It is likely that these differences are caused by inclusion of Breit interaction into the self-consistent field procedure in the MCDHF computations.

4. E1 TRANSITIONS

In this section, we show the results of our calculations of transition probabilities. The transition data computed for Pr II, Pm II, Sm II, Eu II, and Gd II are given in machine-readable format in Tables 10, 11, 12, 13, and 14. The tables include identification of upper and lower levels in LSJ coupling, transition energy, wavelength, line strength, weighted oscillator strength, and transition probabilities in length form. The num-

bers of transitions are 411 314, 7 104 005, 4 720 626, 467 724 (plus 13 154 transitions with Rydberg states, 480 878 in total), and 1 383 694 for Pr II, Pm II, Sm II, Eu II, and Gd II, respectively.

In the following sections, we compare the calculated transition probabilities with available data, except for Pm and Sm for which enough data are not available ¹.

¹ For Sm II, there are transitions probabilities for 7 lines in the NIST database. Unfortunately upper levels do not have clear identification of the configuration. Xu et al. (2003) have performed radiative lifetime measurements with time-resolved laser induced fluorescence (LIF) techniques for 47 levels and have performed relativistic Hartree-Fock (HFR) computations over the energy range 21 000 - 36 000 cm^{-1} , but again the identification of these levels is unclear. Large amount of data (958 lines) have been measured with the same method (Lawler et al. 2006), but all upper levels do not have clear identification. Lifetimes of 82 levels in range 21 655.420 - 29 591.120 cm^{-1} were investigated beam-laser method and transition probabilities were calculated using branching ratios for 35 transitions by Scholl et al. (2002b).

Table 8. Energy Levels (in cm^{-1}) Relative to the Ground State for the States of Gd II.

No.	label	J	P	E
1	$4f^7(8S) 5d^9D6s^1D$	5/2	—	0.00
2	$4f^7(8S) 5d^9D6s^1D$	7/2	—	225.02
3	$4f^7(8S) 5d^9D6s^1D$	9/2	—	536.90
4	$4f^7(8S) 5d^9D6s^1D$	11/2	—	959.98
5	$4f^7(8S) 5d^9D6s^1D$	13/2	—	1536.81
6	$4f^7(8S) 5d^2(3F)^1F$	3/2	—	3026.08
7	$4f^7(8S) 5d^2(3F)^1F$	5/2	—	3173.49
8	$4f^7(8S) 5d^2(3F)^1F$	7/2	—	3382.26
9	$4f^7(8S) 5d^2(3F)^1F$	9/2	—	3654.80
10	$4f^7(8S) 5d^9D6s^8D$	3/2	—	3767.49
11	$4f^7(8S) 5d^9D6s^8D$	5/2	—	3965.84
12	$4f^7(8S) 5d^2(3F)^1F$	11/2	—	3994.44
13	$4f^7(8S) 5d^9D6s^8D$	7/2	—	4269.62
14	$4f^7(8S) 5d^2(3F)^1F$	13/2	—	4405.08
15	$4f^7(8S) 5d^9D6s^8D$	9/2	—	4713.57
16	$4f^7(8S) 5d^2(3F)^1F$	15/2	—	4888.14
17	$4f^7(8S) 5d^9D6s^8D$	11/2	—	5359.77
18	$4f^7(8S) 6s^2^8S$	7/2	—	5713.88
19	$4f^8(7F) 6s^8F$	13/2	+	7507.66
20	$4f^8(7F) 6s^8F$	11/2	+	8691.73

NOTE— Table 8 is published in its entirety in the machine-readable format. Part of the values are shown here for guidance regarding its form and content.

4.1. Pr II

For Pr II, rather rich data are available in the NIST database. Therefore, it can be used as evaluation of our calculations. Comparison between the calculated E1 transitions probabilities and those in the NIST database is presented in Figure 6. Figure 6 includes transitions between $4f^3 6s$ and $4f^3 6p$ and transitions between $4f^3 6p$ and $4f^3 5d$ with clear level identification. The same transitions in length and velocity form are connected with dashed lines. Transitions in the NIST database are based on FT spectroscopy by Ivarsson et al. (2001) and measurements of branching fractions with use of a laser/fast-ion-beam method by Li et al. (2007) and lifetimes determined in a previous study with beam-laser method (Scholl et al. 2002a).

We find that transition probabilities calculated in two forms agree better for the transitions between $4f^3 6s$ and $4f^3 6p$ than those between $4f^3 6p$ and $4f^3 5d$. Compared with the data by other authors, our transitions

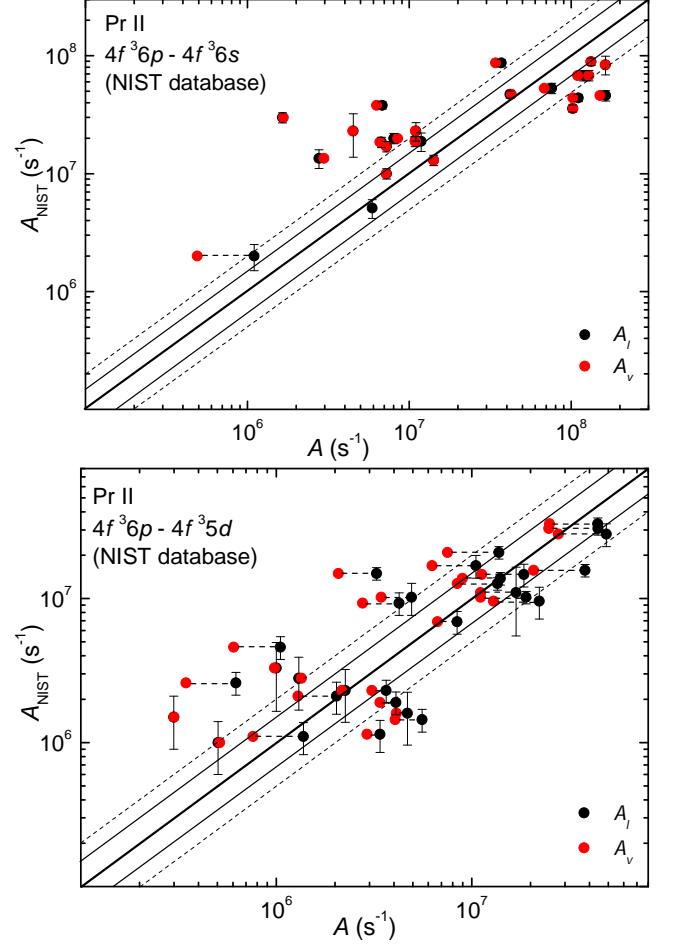


Figure 6. Comparison of transition probability between states of configurations $4f^3 6s - 4f^3 6p$ and between states of configurations $4f^3 6p$ and $4f^3 5d$ for Pr II. The top and bottom panels show a comparison between our results and results from the NIST database. The thick line corresponds to perfect agreement, while the thin solid and dashed lines correspond to deviations by factors of 1.5 and 2.0, respectively. The black and reds points show the values calculated with the length (Babushkin) and velocity (Coulomb) forms, respectively.

in velocity form gives a better agreement in the strong transition area. Therefore, hereafter we show transition probabilities computed in velocity form.

As for the transition wavelength, our calculations give a good agreement with the NIST data. Averaged agreement in the transition wavelength is 2% for the transitions between states of configurations $4f^3 6s$ and $4f^3 6p$, and 4% for the transitions between states of configurations $4f^3 6p$ and $4f^3 5d$ (see Figure 7).

4.2. Eu II

The NIST database presents 13 lines with transition probabilities which are compared with our calculations in Figure 8. There is a very good agreement of transi-

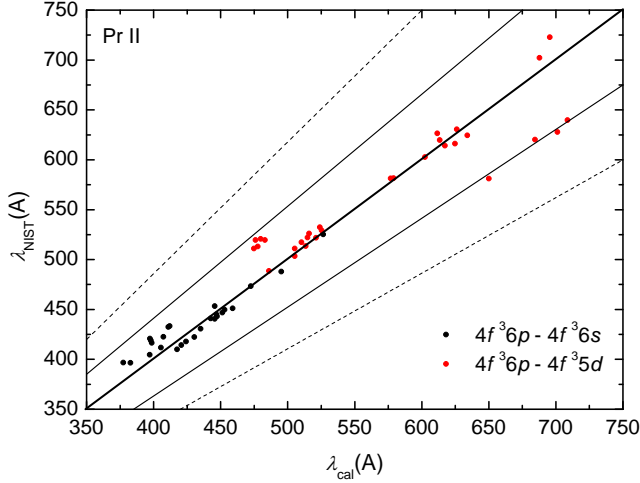


Figure 7. Comparison of transition wavelengths for Pr II between our results (λ_{cal}) and NIST database recommended values (λ_{NIST}). The thick line corresponds to perfect agreement, while thin solid and dashed lines correspond to 10% and 20% deviations.

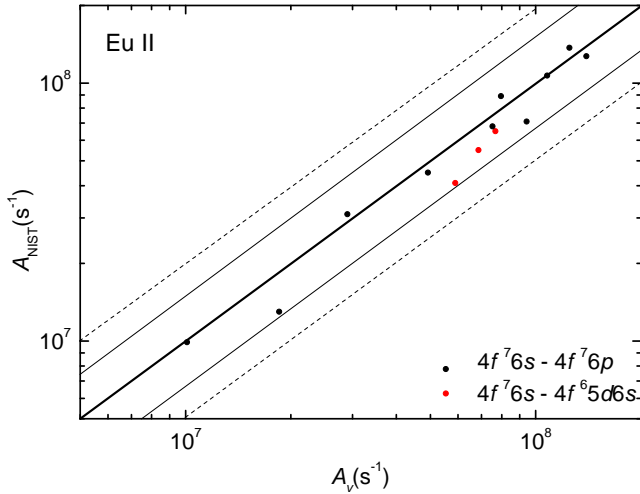


Figure 8. Comparison of transition probability of Eu II between our results (A_v) and NIST database. The thick line corresponds to perfect agreement, while the thin solid and dashed lines correspond to deviations by factors of 1.5 and 2.0, respectively. Transition probabilities are presented in the velocity (Coulomb) form.

tions probabilities although the agreement in the transition wavelength is rather poor, about 14%.

It is worth comparing our results with more available measurements although the data are not always critically evaluated. Summary of experiments for Eu II is given in Table 9. Absolute transition probabilities are measured experimentally through the measurements of lifetimes (τ) and branching fractions (BF) by other authors. Measurements for the lifetime are done using

Table 9. Summary of Experiments on Eu II.

References	N_τ	Method $_\tau$	Method $_{BF}$	N_L
Biemont et al. (1982)	—	TR-LIF	HCL	27
Zhang et al. (2000)	9	TR-LIF	HCL	31
Lawler et al. (2001)	6	TR-LIF	FTS	24
Wang et al. (2013)	30	TR-LIF	HCL	18
Tian et al. (2019)	11	TR-LIF	HCL	24

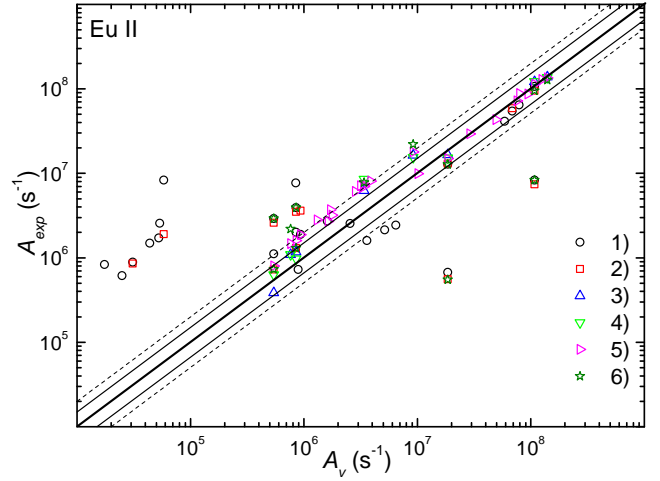


Figure 9. Comparison of transition probability of Eu II between our results (A_v) and data of other authors (A_{exp}): 1) Zhang et al. (2000); 2) Komarovskii (1991); 3) Tian et al. (2019); 4) Wang et al. (2013); 5) Lawler et al. (2001); 6) Karner et al. (1982) and Biemont et al. (1982). The thick line corresponds to perfect agreement, while the thin solid and dashed lines correspond to deviations by factors of 1.5 and 2.0, respectively. Transition probabilities are presented in the velocity (Coulomb) form.

time-resolved laser-induced fluorescence (TR-LIF) while branching factors are estimated from emission spectra of a hollow-cathode discharge lamp with Eu powder in the cathode (HCL) or Fourier transform spectrometer (FTS) data. Table 9 includes the methods as well as the number of lifetimes measurements N_τ and the number of lines N_L .

Comparison with these measurement is given in Figure 9. In this figure, only the levels with clear identifications are included. The most transitions are in the ranges of dashed lines showing the deviation by a factor of 2.0. However, we observe a relatively large deviation in the weak transitions: our calculations give a much smaller transition probabilities than those estimated from the experiments. This may suggest that our strategy of computations is not good enough for weak

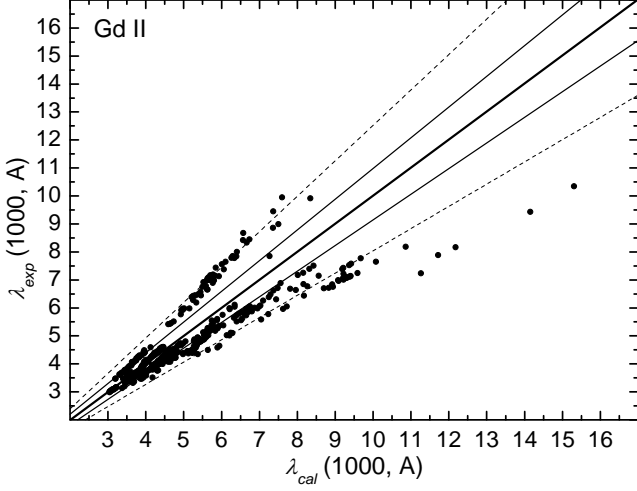


Figure 10. Comparison of transition wavelengths for Gd II between our results and experimental data by Hartog et al. (2006). The thick line corresponds to perfect agreement, while thin solid and dashed lines correspond to 10% and 20% deviations.

transitions. Another possible reason is that transitions other than E1, which we do not include in our calculations, may contribute to these weak lines.

4.3. Gd II

For Gd II, transition probabilities are not presented in the NIST database (Kramida et al. 2018). However, there are several experimental works to address the transition probabilities. For example, experimental transition probabilities are estimated by Corliss & Bozman (1962). Also, Wang et al. (1971) have experimentally measured branching fractions of 12 levels for Gd II using the emission spectrum of a hollow cathode lamp. As a results, transition probabilities for 74 lines of Gd II were derived from a combination of the radiative lifetimes reported in the earlier literature and newly determined branching fractions.

More recently, Hartog et al. (2006) have investigated absolute transition probabilities for 611 lines for Gd II, by using combination of LIF radiative lifetime measurements and branching fraction measurements. Identification of upper and lower energy levels is based on the work by Martin et al. (1978). In Figure 10, wavelengths of 460 transitions from their experiments are compared with our calculations. For comparison, we include only the levels with clear identification. 66% of lines wavelengths are within 10% agreement range (solid lines) and 12% of wavelengths have more than 20% disagreement (dashed lines).

As for the transition probabilities, we obtain reasonable agreement between our computed values and the LIF measurements (Figure 11, colors of the points repre-

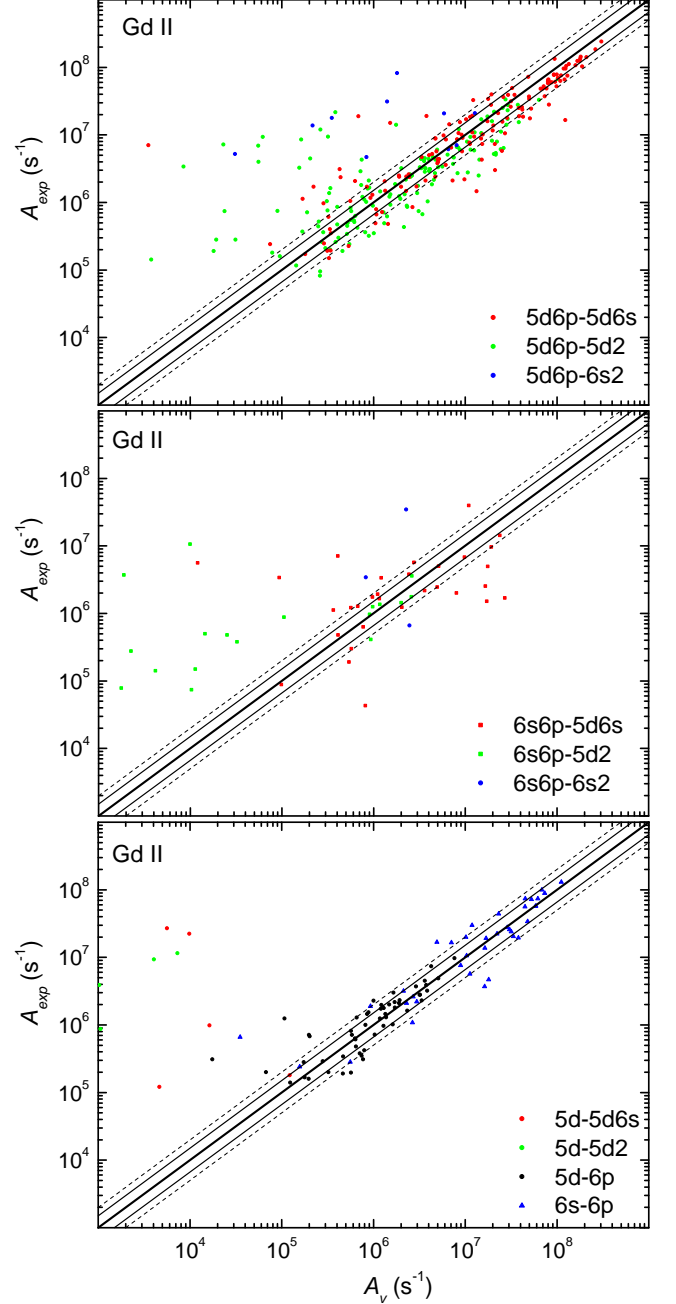


Figure 11. Comparison of transition probability of Gd II between our results (A_v) and the results by Hartog et al. (2006) (A_{exp}). Three panels are divided according to the configurations involved in the transitions. The thick line corresponds to perfect agreement, while the thin solid and dashed lines correspond to deviations by factors of 1.5 and 2.0, respectively. Transition probabilities are presented in the velocity (Coulomb) form.

Table 10. Transition Energies ΔE (in cm^{-1}), Transition Wavelengths λ (in \AA), Line Strengths S (in a.u.), Weighted Oscillator Strengths gf , and Transition Rates A (in s^{-1}) for E1 Transitions of the Pr II ion.

Lower state	Upper state	ΔE (cm^{-1})	λ (\AA)	S	gf	A (s^{-1})	dT
$4f^2(3H)5d^2(3F)5D_1$	$4f^3(4F)5d5D_0$	2769	36101	1.197D-01	1.007D-03	5.157D+03	0.872
$4f^2(3H)5d^2(3F)5F_1$	$4f^3(4F)5d5D_0$	553	180550	5.998D-02	1.009D-04	2.065D+01	0.997
$4f^3(4F)5d5D_0$	$4f^2(3F)5d^2(3F)5F_1$	936	106828	2.116D-01	6.018D-04	1.172D+02	0.266
$4f^3(4F)5d5D_0$	$4f^2(3H)5d^2(3F)3D_1$	1618	61775	6.203D-03	3.050D-05	1.777D+01	0.972
$4f^3(4F)5d5D_0$	$4f^2(3F)5d^2(3F)3P_1$	2826	35384	4.636D-03	3.979D-05	7.067D+01	0.992
$4f^3(4F)5d5D_0$	$4f^2(3F)5d^2(3F)5P_1$	3885	25734	6.263D-02	7.393D-04	2.482D+03	0.857
$4f^3(4F)5d5D_0$	$4f^2(3F)5d^2(3F)5D_1$	4313	23184	1.093D-02	1.432D-04	5.927D+02	0.915
$4f^3(4F)5d5D_0$	$4f^2(3F)5d^2(3F)5P_1$	4739	21100	5.712D-02	8.223D-04	4.106D+03	0.854
$4f^3(4F)5d5D_0$	$4f^2(3F)5d^2(3F)3S_1$	6623	15096	2.818D-03	5.670D-05	5.532D+02	0.395
$4f^3(4F)5d5D_0$	$4f^2(1G)5d^2(3F)3D_1$	7603	13151	5.877D-03	1.357D-04	1.745D+03	0.883
$4f^3(4F)5d5D_0$	$4f^2(3F)5d^2(3F)1P_1$	7933	12604	3.494D-03	8.422D-05	1.178D+03	0.349
$4f^3(4F)5d5D_0$	$4f^2(3F)5d^2(3P)5F_1$	8216	12171	3.326D-03	8.300D-05	1.245D+03	0.964
$4f^3(4F)5d5D_0$	$4f^2(3F)5d^2(1D)3P_1$	8397	11908	8.419D-03	2.147D-04	3.367D+03	0.148
$4f^3(4F)5d5D_0$	$4f^2(3F)5d^2(3F)3D_1$	8690	11507	4.930D-04	1.301D-05	2.185D+02	0.965
$4f^3(4F)5d5D_0$	$4f^2(1G)5d^2(3F)3P_1$	11098	9010	1.194D-03	4.027D-05	1.102D+03	0.577
$4f^3(4F)5d5D_0$	$4f^2(3F)5d^2(3P)5D_1$	12485	8009	7.617D-03	2.888D-04	1.001D+04	0.750
$4f^3(4F)5d5D_0$	$4f^2(3F)5d^2(1G)3P_1$	12982	7702	3.509D-03	1.383D-04	5.186D+03	0.992
$4f^3(4F)5d5D_0$	$4f^2(3H)5d^2(1G)3D_1$	13084	7642	5.366D-03	2.133D-04	8.119D+03	0.234
$4f^3(4F)5d5D_0$	$4f^2(3F)5d^2(3P)3D_1$	14340	6973	9.093D-05	3.961D-06	1.811D+02	0.991
$4f^3(4F)5d5D_0$	$4f^2(3H)5d^2(1G)3P_1$	15904	6287	4.553D-03	2.199D-04	1.237D+04	0.993

NOTE— Table 10 is published in its entirety in the machine-readable format. All transition data are in length form. Part of the values are shown here for guidance regarding its form and content.

sent different configurations). In this figure, we include transitions with transition probabilities higher than 10^3 from Hartog et al. (2006). At closer look, however, there is disagreement in particular for the two-electron-one-photon transitions between states of configurations $4f^75d6p$ and $4f^76s^2$ and $4f^76s6p$ and $4f^75d^2$. Our calculations underestimate the experimental values of these transitions. These transitions are due to mixing of configurations in the ASFs which allows one-electron-one-photon transitions (with one electron jump and $\Delta l \pm 1$). The calculated values can be changed significantly by a subtle change in degrees of mixing of the allowed configurations in the ASFs. On the other hand, agreement with Hartog et al. (2006) is much better for strong transitions.

5. SUMMARY

We presented *ab-initio* atomic calculations of energy levels and E1 transitions from Pr II to Gd II ions based on the strategy developed for the calculations of Nd II (Gaigalas et al. 2019). In total 2 145, 9 774, 8 393,

2 473, and 4 397 levels are presented for Pr II, Pm II, Sm II, Eu II, and Gd II, respectively. Some of the Rydberg states are also included to the computations for Eu II. By comparing with the NIST database and the results by other authors, we confirmed that our calculations achieve good accuracy. For the energy levels, the averaged accuracy compared with the NIST data are 8%, 12%, 6%, 8%, and 7% for Pr II, Pm II, Sm II, Eu II, and Gd II, respectively. These are the highest accuracies achieved for this kind of complete atomic calculations needed for opacity calculations. There is no clear dependence of accuracy on atomic number Z . This means that data of lanthanide set can be computed in similar way to the isoelectronic sequence. By using the results of atomic structure calculations, E1 transitions between levels are computed. We provide data for 411 314, 7 104 005, 4 720 626, 467 724, and 1 383 694 transitions for Pr II, Pm II, Sm II, Eu II, and Gd II, respectively. Transition probabilities are compared with NIST database as well as the results of other works. Our computed E1 type transition probabilities are in good

Table 11. Transition Energies ΔE (in cm^{-1}), Transition Wavelengths λ (in \AA), Line Strengths S (in a.u.), Weighted Oscillator Strengths gf , and Transition Rates A (in s^{-1}) for E1 Transitions of the Pm II ion.

Lower state	Upper state	ΔE (cm^{-1})	λ (\AA)	S	gf	A (s^{-1})	dT
$4f^5(6H) 5d^7F_0$	$4f^4(5I) 5d^2(3F) ^7G_1$	7085	14112	1.596D-02	3.435D-04	3.835D+03	0.986
$4f^5(6H) 5d^7F_0$	$4f^4(5I) 5d^2(3F) ^7F_1$	10754	9298	4.139D-01	1.352D-02	3.477D+05	0.612
$4f^5(6H) 5d^7F_0$	$4f^4(5I) 5d^2(3F) ^5F_1$	12200	8196	1.145D-01	4.245D-03	1.405D+05	0.670
$4f^5(6H) 5d^7F_0$	$4f^4(5I) 5d^2(1G) ^5D_1$	18581	5381	4.990D-10	2.816D-11	2.162D-03	1.000
$4f^5(6H) 5d^7F_0$	$4f^4(5S) 5d^2(3F) ^7F_1$	19182	5213	6.356D-03	3.703D-04	3.030D+04	0.962
$4f^5(6H) 5d^7F_0$	$4f^4(5I) 5d^2(1G) ^5F_1$	20262	4935	5.274D-05	3.246D-06	2.963D+02	0.738
$4f^5(6H) 5d^7F_0$	$4f^4(5I) 5d^2(3F) ^7G_1$	20827	4801	2.122D-03	1.342D-04	1.295D+04	0.943
$4f^5(6H) 5d^7F_0$	$4f^4(5I) 5d^2(3F) ^7D_1$	22329	4478	2.629D-02	1.783D-03	1.977D+05	0.619
$4f^5(6H) 5d^7F_0$	$4f^4(5I) 5d^2(3F) ^7F_1$	22721	4401	8.370D-02	5.777D-03	6.632D+05	0.426
$4f^5(6H) 5d^7F_0$	$4f^4(5F) 5d^2(3F) ^5F_1$	24509	4080	1.207D-03	8.991D-05	1.200D+04	0.521
$4f^5(6H) 5d^7F_0$	$4f^4(5F) 5d^2(3P) ^7G_1$	25471	3926	3.671D-02	2.840D-03	4.097D+05	0.240
$4f^5(6H) 5d^7F_0$	$4f^4(5S) 5d^2(3F) ^5F_1$	26213	3814	6.045D-04	4.814D-05	7.354D+03	0.736
$4f^5(6H) 5d^7F_0$	$4f^4(5I) 5d^2(1D) ^5P_1$	26337	3796	7.825D-06	6.260D-07	9.656D+01	0.927
$4f^5(6H) 5d^7F_0$	$4f^4(5I) 5d^2(1D) ^5P_1$	26949	3710	7.221D-06	5.911D-07	9.545D+01	0.994
$4f^5(6H) 5d^7F_0$	$4f^4(5I) 5d^2(1D) ^5D_1$	27588	3624	5.019D-04	4.206D-05	7.118D+03	0.864
$4f^5(6H) 5d^7F_0$	$4f^4(5I) 5d^2(3P) ^7D_1$	28134	3554	1.602D-02	1.369D-03	2.409D+05	0.259
$4f^5(6H) 5d^7F_0$	$4f^4(5F) 5d^2(3F) ^5D_1$	28353	3526	8.565D-03	7.376D-04	1.318D+05	0.111
$4f^5(6H) 5d^7F_0$	$4f^4(5I) 5d^2(3P) ^7F_1$	28610	3495	2.125D-03	1.846D-04	3.361D+04	0.786
$4f^5(6H) 5d^7F_0$	$4f^4(5I) 5d^2(3P) ^7F_1$	29032	3444	1.239D-02	1.093D-03	2.048D+05	0.553
$4f^5(6H) 5d^7F_0$	$4f^4(5I) 5d^2(3F) ^5P_1$	29210	3423	2.067D-02	1.834D-03	3.480D+05	0.216

NOTE— Table 11 is published in its entirety in the machine-readable format. All transition data are in length form. Part of the values are shown here for guidance regarding its form and content.

agreement with presented in NIST database experimental values, especially in the area of strong transitions.

This research was funded by a grant (No. S-LJB-18-1) from the Research Council of Lithuania. This research was also supported by the JSPS Bilateral Joint Research

Project. D.K. is grateful for the support by the NINS program of Promoting Research by Networking among Institutions (grant No. 01411702). The computations presented in this paper were performed at the High Performance Computing Center "HPC Sauletekis" of the Faculty of Physics at Vilnius University.

REFERENCES

- Abbott, B. P., Abbott, R., Abbott, T. D., et al. 2017, ApJL, 848, L12
- Ahmad, S. A., Venugopalan, A., & Saksena, G. D. 1979, Spectrochim. Acta, Part B, 34, 221
- Akhtar, N., & Windholz, L. 2019, J. Phys. B: At. Mol. Opt. Phys., 240, 29
- Albertson, W. 1934, Phys. Rev., 45, 499
- . 1936, Astrophys. J., 84, 26
- Albertson, W. E., Bruynes, H., & Hanau, R. 1940, Phys. Rev., 57, 292
- Barnes, J., & Kasen, D. 2013, ApJ, 775, 18
- Biemont, E., Karner, C., Meyer, G., Traeger, F., & Zu Putnitz, G. 1982, Astronomy and Astrophysics, 107, 166
- Blaise, J., Morillon, C., Schweighofer, M.-G., & Verges, J. 1969, Spectrochim. Acta, Part B, 24, 405
- Blaise, J., Van Kleef, T. A. M., & Wyart, J. F. 1971, J. Phys. (Paris), 32, 617
- Blaise, J., Verges, J., Wyart, J. F., & Zalubas, R. 1973, J. Opt. Soc. Am., 63, 1315
- Blaise, J., Wyart, J. F., & Camus, P. 1974, Phys. Script., 9, 325
- Brewer, L. 1971, J. Opt. Soc. Am., 61, 1666

Table 12. Transition Energies ΔE (in cm^{-1}), Transition Wavelengths λ (in \AA), Line Strengths S (in a.u.), Weighted Oscillator Strengths gf , and Transition Rates A (in s^{-1}) for E1 Transitions of the Sm II ion.

Lower state	Upper state	ΔE (cm^{-1})	λ (\AA)	S	gf	A (s^{-1})	dT
$4f^6(7F) 5d^8H_{11/2}$	$4f^7(6I) 6I_{11/2}$	34628	2887	2.376D-02	2.499D-03	1.666D+05	0.226
$4f^6(7F) 5d^8H_{11/2}$	$4f^7(6F) 6F_{11/2}$	44272	2258	6.084D-03	8.182D-04	8.914D+04	0.278
$4f^6(7F) 5d^8H_{11/2}$	$4f^7(6F) 6F_{11/2}$	47585	2101	6.743D-06	9.747D-07	1.226D+02	0.881
$4f^6(7F) 5d^8H_{11/2}$	$4f^7(4H) 4H_{11/2}$	51906	1926	5.479D-06	8.638D-07	1.293D+02	0.373
$4f^6(7F) 5d^8H_{11/2}$	$4f^7(4H) 4H_{11/2}$	52021	1922	1.221D-04	1.929D-05	2.902D+03	0.475
$4f^6(7F) 5d^8H_{11/2}$	$4f^7(4H) 4H_{11/2}$	52375	1909	5.185D-05	8.249D-06	1.257D+03	0.050
$4f^6(7F) 5d^8H_{11/2}$	$4f^7(4K) 4K_{11/2}$	54211	1844	1.917D-05	3.157D-06	5.158D+02	0.994
$4f^6(7F) 5d^8H_{11/2}$	$4f^7(4H) 4H_{11/2}$	55780	1792	8.194D-04	1.388D-04	2.401D+04	0.121
$4f^6(7F) 5d^8H_{11/2}$	$4f^7(4H) 4H_{11/2}$	56367	1774	1.286D-04	2.203D-05	3.891D+03	0.228
$4f^6(7F) 5d^8H_{11/2}$	$4f^7(4G) 4G_{11/2}$	56877	1758	1.260D-04	2.177D-05	3.915D+03	0.243
$4f^6(7F) 5d^8H_{11/2}$	$4f^7(4G) 4G_{11/2}$	58572	1707	8.167D-07	1.453D-07	2.771D+01	0.697
$4f^6(7F) 5d^8H_{11/2}$	$4f^7(4G) 4G_{11/2}$	58814	1700	7.015D-05	1.253D-05	2.409D+03	0.470
$4f^6(7F) 5d^8H_{11/2}$	$4f^7(4I) 4I_{11/2}$	59094	1692	2.094D-05	3.759D-06	7.297D+02	0.950
$4f^6(7F) 5d^8H_{11/2}$	$4f^7(4I) 4I_{11/2}$	61660	1621	9.523D-05	1.783D-05	3.769D+03	0.167
$4f^6(7F) 5d^8H_{11/2}$	$4f^7(4K) 4K_{11/2}$	62829	1591	5.517D-04	1.052D-04	2.310D+04	0.156
$4f^6(7F) 5d^8D_{11/2}$	$4f^7(6I) 6I_{11/2}$	31992	3125	2.834D-03	2.754D-04	1.567D+04	0.545
$4f^6(7F) 5d^8D_{11/2}$	$4f^7(6F) 6F_{11/2}$	41636	2401	3.545D-02	4.483D-03	4.320D+05	0.939
$4f^6(7F) 5d^8D_{11/2}$	$4f^7(6F) 6F_{11/2}$	44949	2224	6.156D-02	8.405D-03	9.440D+05	0.921
$4f^6(7F) 5d^8D_{11/2}$	$4f^7(4H) 4H_{11/2}$	49270	2029	1.859D-04	2.782D-05	3.755D+03	0.717
$4f^6(7F) 5d^8D_{11/2}$	$4f^7(4H) 4H_{11/2}$	49385	2024	2.738D-03	4.107D-04	5.568D+04	0.862

NOTE— Table 12 is published in its entirety in the machine-readable format. All transition data are in length form. Part of the values are shown here for guidance regarding its form and content.

- Corliss, C. H., & Bozman, W. R. 1962, Experimental Transition Probabilities for Spectral Lines of Seventy Elements (Washington: US GPO)
- Cowan, R. 1981, The Theory of Atomic Structure and Spectra (University of California Press, Berkeley, CA)
- Ekman, J., Jönsson, P., Gustafsson, S., et al. 2014, Astronomy and Astrophysics, A24, 564
- Fischer, C. F., Godefroid, M., Brage, T., Jönsson, P., & Gaigalas, G. 2016, Journal of Physics B: Atomic, Molecular and Optical Physics, 49, 182004
- Fontes, C. J., Fryer, C. L., Hungerford, A. L., et al. 2017, arXiv:1702.02990, arXiv:1702.02990
- Fritzsche, S., & Grant, I. 1994, Physics Letters A, 186, 152
- Furmann, B., & Stefańska, D. 2013, J. Phys. B: At. Mol. Opt. Phys., 46, 235005
- Furmann, B., Stefańska, D., Dembczyński, J., & Stachowska, E. 2005, Physica Scripta, 72, 300
- . 2007, Atomic Data and Nuclear Data Tables, 93, 127
- Furmann, B., Stefańska, D., Stachowska, E., Ruczkowska, J., & Dembczyński, J. 2001, Eur. Phys. J. D, 17, 275
- Gaigalas, G., Fischer, C., Rynkun, P., & Jönsson, P. 2017, Atoms, 5, 6
- Gaigalas, G., Kato, D., Rynkun, P., Radžiūtė, L., & Tanaka, M. 2019, The Astrophysical Journal Supplement Series, 240, 29
- Gaigalas, G., & Rudzikas, Z. 1996, Journal of Physics B: Atomic, Molecular and Optical Physics, 29, 3303
- Gaigalas, G., & Rudzikas, Z. 1998, Atomic Data and Nuclear Data Tables, 70, 139
- Gaigalas, G., Rudzikas, Z., & Fischer, C. F. 1997, Journal of Physics B: Atomic, Molecular and Optical Physics, 30, 3747
- Ginibre, A. 1989a, Physica Scripta, 39, 694
- . 1989b, Physica Scripta, 39, 710
- Grant, I. P. 1974, Journal of Physics B: Atomic and Molecular Physics, 7, 1458
- . 2007, Relativistic Quantum Theory of Atoms and Molecules (Springer, New York)

Table 13. Transition Energies ΔE (in cm^{-1}), Transition Wavelengths λ (in \AA), Line Strengths S (in a.u.), Weighted Oscillator Strengths gf , and Transition Rates A (in s^{-1}) for E1 Transitions of the Eu II ion.

Lower state	Upper state	ΔE (cm^{-1})	λ (\AA)	S	gf	A (s^{-1})	dT
$4f^7(6P)5d\ ^7F_0$	$4f^8(7F) \ ^7F_1$	9040	11061	1.303D-03	3.579D-05	6.504D+02	0.840
$4f^7(6P)5d\ ^7F_0$	$4f^8(5D) \ ^5D_1$	30106	3321	2.056D-02	1.880D-03	3.789D+05	0.794
$4f^7(6P)5d\ ^7F_0$	$4f^8(5F) \ ^5F_1$	36281	2756	1.696D-03	1.869D-04	5.472D+04	0.992
$4f^7(6P)5d\ ^7F_0$	$4f^8(5F) \ ^5F_1$	36869	2712	1.379D-03	1.544D-04	4.668D+04	0.765
$4f^7(6P)5d\ ^7F_0$	$4f^8(5F) \ ^5F_1$	37397	2673	3.813D-03	4.332D-04	1.347D+05	0.714
$4f^7(6P)5d\ ^5D_0$	$4f^8(7F) \ ^7F_1$	2361	42339	1.176D-03	8.438D-06	1.046D+01	0.962
$4f^7(6P)5d\ ^5D_0$	$4f^8(5D) \ ^5D_1$	23427	4268	1.070D-03	7.619D-05	9.298D+03	0.231
$4f^7(6P)5d\ ^5D_0$	$4f^8(5F) \ ^5F_1$	29602	3378	2.478D-02	2.228D-03	4.342D+05	0.363
$4f^7(6P)5d\ ^5D_0$	$4f^8(5F) \ ^5F_1$	30191	3312	5.379D-02	4.933D-03	9.998D+05	0.579
$4f^7(6P)5d\ ^5D_0$	$4f^8(5F) \ ^5F_1$	30718	3255	5.116D-02	4.773D-03	1.001D+06	0.980
$4f^8(7F) \ ^7F_1$	$4f^7(6D)5d\ ^7F_0$	1158	86316	2.027D-02	7.135D-05	6.388D+01	0.982
$4f^7(6D)5d\ ^7F_0$	$4f^8(5D) \ ^5D_1$	19907	5023	6.089D-03	3.681D-04	3.244D+04	0.891
$4f^7(6D)5d\ ^7F_0$	$4f^8(5F) \ ^5F_1$	26082	3833	7.236D-01	5.733D-02	8.671D+06	0.880
$4f^7(6D)5d\ ^7F_0$	$4f^8(5F) \ ^5F_1$	26670	3749	1.442D-02	1.168D-03	1.848D+05	0.970
$4f^7(6D)5d\ ^7F_0$	$4f^8(5F) \ ^5F_1$	27198	3676	1.119D-01	9.245D-03	1.520D+06	0.847
$4f^8(7F) \ ^7F_1$	$4f^7(6D)5d\ ^5D_0$	5664	17653	9.848D-04	1.694D-05	3.627D+02	0.914
$4f^7(6D)5d\ ^5D_0$	$4f^8(5D) \ ^5D_1$	15400	6493	2.752D-02	1.287D-03	6.791D+04	0.063
$4f^7(6D)5d\ ^5D_0$	$4f^8(5F) \ ^5F_1$	21576	4634	6.207D-02	4.068D-03	4.211D+05	0.731
$4f^7(6D)5d\ ^5D_0$	$4f^8(5F) \ ^5F_1$	22164	4511	3.348D-02	2.254D-03	2.462D+05	0.022
$4f^7(6D)5d\ ^5D_0$	$4f^8(5F) \ ^5F_1$	22692	4406	4.103D-01	2.828D-02	3.238D+06	0.942

NOTE— Table 13 is published in its entirety in the machine-readable format. All transition data are in length form. Part of the values are shown here for guidance regarding its form and content.

Hartog, E. A. D., Lawler, J. E., Sneden, C., & Cowan, J. J. 2006, The Astrophysical Journal Supplement Series, 167, 292

Indelicato, P., Santos, J., Boucard, S., & Desclaux, J.-P. 2007, Eur. Phys. J. D, 45, 155

Ivarsson, S., Litzén, U., & Wahlgren, G. M. 2001, Physica Scripta, 64, 455

Jönsson, P., Gaigalas, G., Bieroń, J., Fischer, C. F., & Grant, I. 2013, Computer Physics Communications, 184, 2197

Karner, C., Meyer, G., Traeger, F., & Zu Putlitz, G. 1982, Astronomy and Astrophysics, 107, 161

Kasen, D., Badnell, N. R., & Barnes, J. 2013, ApJ, 774, 25

Komarovskii, V. A. 1991, Opt. Spectrosc. (USSR), 71, 322

Kramida, A., Yu. Ralchenko, Reader, J., & and NIST ASD Team. 2018, NIST Atomic Spectra Database (ver. 5.5.6), [Online]. Available: <https://physics.nist.gov/asd> [2018, May 29]. National Institute of Standards and Technology, Gaithersburg, MD., ,

Lawler, J. E., Den Hartog, E. A., Sneden, C., & Cowan, J. J. 2006, The Astrophysical Journal Supplement Series, 162, 227260

Lawler, J. E., Wickliffe, M. E., & Den Hartog, E. A. 2001, THE ASTROPHYSICAL JOURNAL, 563, 1075

Li, R., Chatelain, R., Holt, R. A., et al. 2007, Phys. Scr., 76, 577

Martin, W. C. 1971, J. Opt. Soc. Am., 167, 292

Martin, W. C., Zalubas, R., & Hagan, L. 1978, Atomic Energy Levels The Rare-Earth Elements (Nat. Bur. Stand., U.S.)

Olsen, J., Godefroid, M. R., Jönsson, P., Malmqvist, P. A., & Fischer, C. F. 1995, Phys. Rev. E, 52, 4499

Ottot, R., Hühnermann, H., Reader, J., & Wyart, J.-F. 1995, J. Phys. B: At. Mol. Opt. Phys., 28, 3615

Radžiūtė, L., Gaigalas, G., Kato, D., et al. 2015, J. Quant. Spectrosc. Radiat. Transf., 152, 94

Rao, P. M., Ahmad, S. A., Venugopalan, A., & Saksena, G. D. 1990, Z. Phys. D, 15, 211

Table 14. Transition Energies ΔE (in cm^{-1}), Transition Wavelengths λ (in \AA), Line Strengths S (in a.u.), Weighted Oscillator Strengths gf , and Transition Rates A (in s^{-1}) for E1 Transitions of the Gd II ion.

Lower state	Upper state	ΔE (cm^{-1})	λ (\AA)	S	gf	A (s^{-1})	dT
$4f^7({}^8S)5d^9D6s^1D_{11/2}$	$4f^8({}^7F)6s^8F_{11/2}$	7731	12933	1.622D-06	3.809D-08	1.265D-01	0.994
$4f^7({}^8S)5d^9D6s^1D_{11/2}$	$4f^8({}^7F)6s^6F_{11/2}$	8671	11531	3.131D-07	8.247D-09	3.447D-02	0.998
$4f^7({}^8S)5d^9D6s^1D_{11/2}$	$4f^8({}^5G)6s^6G_{11/2}$	33824	2956	1.511D-06	1.552D-07	9.875D+00	0.031
$4f^7({}^8S)5d^9D6s^1D_{11/2}$	$4f^8({}^5G)6s^4G_{11/2}$	34708	2881	1.063D-06	1.121D-07	7.510D+00	0.161
$4f^7({}^8S)5d^9D6s^1D_{11/2}$	$4f^8({}^5L)6s^6L_{11/2}$	35251	2836	9.906D-09	1.060D-09	7.327D-02	0.508
$4f^7({}^8S)5d^9D6s^1D_{11/2}$	$4f^8({}^5H)6s^6H_{11/2}$	39556	2528	1.645D-08	1.976D-09	1.719D-01	0.710
$4f^7({}^8S)5d^9D6s^1D_{11/2}$	$4f^8({}^5H)6s^4H_{11/2}$	40715	2456	6.683D-09	8.265D-10	7.616D-02	0.669
$4f^7({}^8S)5d^9D6s^1D_{11/2}$	$4f^8({}^5F)6s^6F_{11/2}$	41839	2390	1.807D-07	2.297D-08	2.235D+00	0.803
$4f^7({}^8S)5d^9D6s^1D_{11/2}$	$4f^8({}^5I)6s^6I_{11/2}$	44260	2259	3.334D-11	4.482D-12	4.881D-04	0.915
$4f^7({}^8S)5d^9D6s^1D_{11/2}$	$4f^8({}^5I)6s^4I_{11/2}$	45531	2196	1.077D-09	1.489D-10	1.716D-02	0.275
$4f^7({}^8S)5d^9D6s^1D_{11/2}$	$4f^8({}^5K)6s^6K_{11/2}$	47419	2108	8.083D-08	1.164D-08	1.455D+00	0.426
$4f^7({}^8S)5d^9D6s^1D_{11/2}$	$4f^8({}^5K)6s^4K_{11/2}$	49135	2035	4.864D-08	7.259D-09	9.743D-01	0.161
$4f^7({}^8S)5d^9D6s^1D_{11/2}$	$4f^8({}^5G)6s^6G_{11/2}$	49860	2005	1.753D-07	2.655D-08	3.669D+00	0.641
$4f^7({}^8S)5d^9D6s^1D_{11/2}$	$4f^8({}^5K)6s^4K_{11/2}$	50373	1985	7.274D-08	1.113D-08	1.569D+00	0.924
$4f^7({}^8S)5d^9D6s^1D_{11/2}$	$4f^8({}^5G)6s^4G_{11/2}$	50830	1967	5.492D-08	8.481D-09	1.218D+00	0.933
$4f^7({}^8S)5d^9D6s^1D_{11/2}$	$4f^8({}^5K)6s^4K_{11/2}$	52462	1906	1.719D-06	2.739D-07	4.191D+01	0.711
$4f^7({}^8S)5d^9D6s^1D_{11/2}$	$4f^8({}^5K)6s^4K_{11/2}$	54181	1845	1.796D-10	2.956D-11	4.824D-03	0.992
$4f^7({}^8S)5d^9D6s^1D_{11/2}$	$4f^8({}^3K)6s^4K_{11/2}$	55996	1785	5.269D-12	8.963D-13	1.562D-04	0.982
$4f^7({}^8S)5d^9D6s^1D_{11/2}$	$4f^8({}^3G)6s^4G_{11/2}$	56703	1763	6.780D-08	1.167D-08	2.087D+00	0.920
$4f^7({}^8S)5d^9D6s^1D_{11/2}$	$4f^8({}^5H)6s^6H_{11/2}$	57987	1724	9.638D-09	1.697D-09	3.173D-01	0.574

NOTE— Table 14 is published in its entirety in the machine-readable format. All transition data are in length form. Part of the values are shown here for guidance regarding its form and content.

Rosen, N., Harrison, G. R., & McNally, J. R., J. 1941, Phys. Rev., 60, 722
 Russel, H. N., Albertson, W., & Davis, D. N. 1941, Physical Review, 60, 641
 Scholl, T. J., Holt, R. A., Masterman, D., et al. 2002a, Canadian Journal of Physics, 80, 713
 —. 2002b, Can. J. Phys., 80, 1621
 Spector, N. 1970a, J. Phys. (Paris) Colloques, 31, C4
 —. 1970b, J. Opt. Soc. Am., 60, 763
 Tanaka, M., & Hotokezaka, K. 2013, ApJ, 775, 113
 Tanaka, M., Kato, D., Gaigalas, G., & Sekiguchi, Y. 2019, arXiv:1906.08914, arXiv:1906.08914
 Tanaka, M., Kato, D., Gaigalas, G., et al. 2018, ApJ, 852, 109
 Tian, Y., Wang, X., C., L., Yu, Q., & Dai, Z. 2019, MNRAS, 485, 4485

Vander Sluis, K. L., & Nugent, L. J. 1974, J. Opt. Soc. Am., 64, 687
 Venugopalan, A., Afzal, S., & Ahmad, S. A. 1998, Spectrochimica Acta Part B, 53, 633
 Villemoes, P., M., W., Arnesen, A., Weiler, C., & Wännström, A. 1995, Phys. Rev. A, 51, 2838
 Wang, Q., Shang, X., .Y, T., Fan, S., & Dai, Z. 2013, MNRAS, 435, 2060
 Wang, Q., Yin, J., Jiang, L., et al. 1971, J. Phys. B: At. Mol. Opt. Phys., 61, 1682
 Watson, D., Hansen, C. J., Selsing, J., et al. 2019, arXiv e-prints, arXiv:1910.10510
 Wyart, J. F. 2011, Canadian Journal of Physics, 89(4), 451
 Xu, H. L., Svanberg, S., Quinet, P., Garnir, H. P., & Biémont, E. 2003, J. Phys. B, 36, 4773
 Zhang, Z. G., Li, Z. S., Lundberg, H., et al. 2000, J. Phys. B: At. Mol. Opt. Phys, 30, 521